Ultrafine Nanoporous Aluminum by Electrolytic Dealloying of Aluminum-Magnesium Alloys in Glyme-Based Electrolytes with Recovery of Sacrificial Magnesium

Timothy Lee,[a] Hyeongjun Koh,[a] Alexander K. Ng,[a] Jiaxin Liu, [a] Eric Stach,[a] and Eric Detsi[a,*]

[a] *Department of Materials Science & Engineering, University of Pennsylvania, Philadelphia PA 19104, USA*

* *Email: detsi@seas.upenn.edu*

Abstract: Air-free electrolytic dealloying using non-aqueous electrolytes is a sustainable method for creating nanoporous Al (NP-Al) with highly reactive nanoscale-sized ligaments from Al-Mg parent alloys while simultaneously recovering the sacrificial Mg. However, this synthesis strategy is limited in versatility by the low number of available non-aqueous electrolytes that can conduct Mg ions and has so far only been proven to work with all-phenyl complex (APC) electrolyte derived from *in situ* reaction between two equivalents of Lewis base C_6H_5ClMg and one equivalent of Lewis acid $AlCl_3$ in tetrahydrofuran (THF) solvent. Here we demonstrated that a new electrolyte consisting of $MgCl_2/AlCl_3/Mg(TFSI)_2$ (or MACT) in glyme-based solvents recently introduced in the Mg-ion battery community can also be used to create NP-Al. This alternative electrolyte exhibits higher electrochemical performance than APC and can create ultrafine NP-Al with ≈6-14 nm ligament size, which is smaller than the ≈10-20 nm ligament size commonly achieved using APC.

Key Words: Metal fuel, air-free synthesis, electrolytic dealloying, nanoporous aluminum, recovery of sacrificial materials

Graphical Abstract:

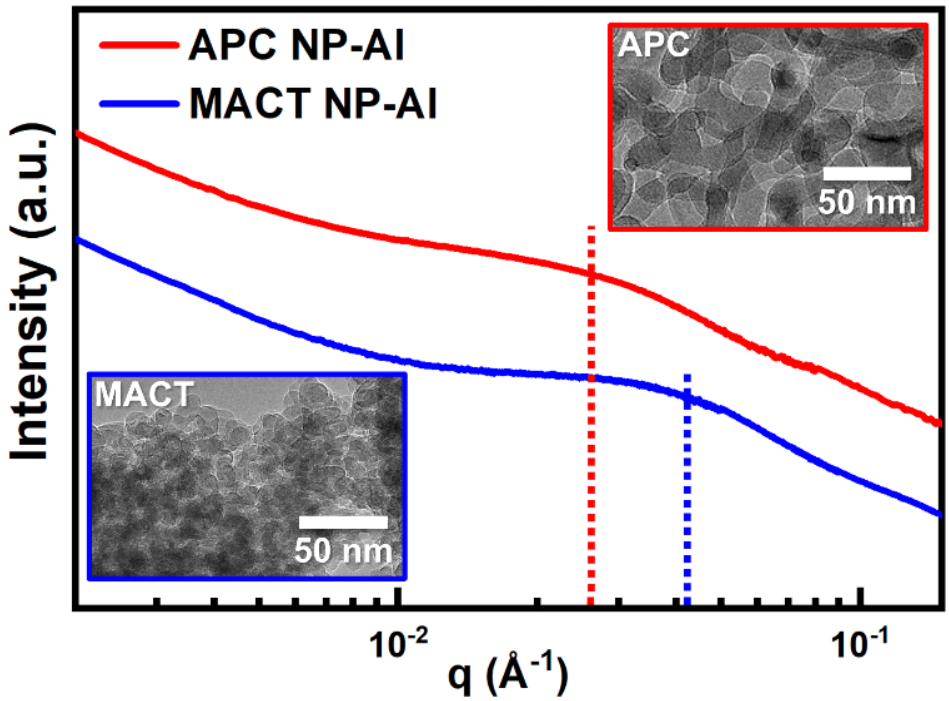

In recent years, selective alloy leaching (or dealloying) has been used to create nanoporous metals for various applications including energy conversion and storage purposes.[1–6] One example is nanoporous aluminum (NP-Al), which has been created by several methods such as air-free electrolytic dealloying under an inert environment using a non-aqueous electrolyte, or galvanic replacement reaction, and has various applications such as hydrogen generation and plasmonics.[5,7] The main principle to create NP-Al in these methods involves creating a binary parent alloy of Al and a sacrificial component such as magnesium (Mg); this parent alloy is then subsequently dealloyed to remove the sacrificial component and to leave behind nanostructured Al with a bicontinuous, nanoporous structure with varying ligament and pore sizes depending on the synthesis method used.[5,7] Electrolytic dealloying under an inert environment is advantageous for several reasons: (i) the sacrificial component used can be recovered at the counter electrode, and reused to create new parent alloys, which promotes the sustainability of this process for large-scale applications,[5] (ii) the NP-Al ligaments produced are nearly oxide free,[5] and (iii) the structure size of NP-Al produced by the state-of-the-art method is ≈10-20 nm, resulting in very high chemical reactivity when exposed to water to produce hydrogen for fuel cell applications.[8]

However, this dealloying method faces drawbacks in experimental flexibility because the number of available Mg-ion conducting electrolytes in the literature is limited. Indeed, the most common non-aqueous electrolyte of choice is 0.4 M all-phenyl complex or "APC" used by the Mg-ion battery community [9–11], which is derived from *in situ* reaction between two equivalents of Lewis base phenylmagnesium chloride (C_6H_5ClMg) and one equivalent of Lewis acid aluminum trichloride ($AlCl_3$) in tetrahydrofuran (THF) solvent. To our knowledge, APC is also the only electrolyte tested so far for air-free electrolytic dealloying with Mg as the sacrificial component.[5] Herein we show how NP-Al can be created via air-free electrolytic dealloying by using a glyme-based Mg-ion conducting electrolyte made of 0.25 M $MgCl_2/AlCl_3/Mg(TFSI)_2$ (1:2:1 molar ratio) in 1,2-dimethoxyethane (DME) solvent called "MACT." This electrolyte was recently developed by Yang *et al.* for use in Mg-sulfur batteries and chosen for its relatively high ionic conductivity (6.82 mS/cm).[12] We also show how this electrolyte can be used to create NP-Al with much finer ligaments and pores compared to APC. Analysis of NP-Al made in both APC as the control

and MACT electrolytes shows that the main advantages of electrolytic dealloying mentioned earlier are still present, including the sustainable recovery of the sacrificial component, and the high reactivity from the nearly oxide-free NP-Al created. This high reactivity was tested by reacting NP-Al created in MACT electrolyte with deionized (DI) H_2O, which undergoes a hydrolysis reaction that can produce hydrogen and various high-temperature alumina byproducts and may have applications in power generation or solid rocket fuel additives.

The performance of both APC and MACT as Mg-ion electrolytes was first investigated to show that both electrolytes can be used for electrolytic dealloying. In doing so, these electrolytes were characterized using electrochemical impedance spectroscopy (EIS) and cyclic voltammetry (CV), as shown in **Figure 1**. EIS is first conducted at OCV for the MACT and APC electrolytes using symmetrical Mg electrodes with geometrical area of 1 cm^2 (**Figure 1a**), The electrolyte resistance (R_Ω) was then estimated from the real axis Z' value to be lower for MACT ($R_\Omega \approx 84\ \Omega$) compared to APC ($R_\Omega \approx 116\ \Omega$). Next, the charge-transfer resistance (R_{CT}) at OCV estimated from the semi-circle diameter was found to be much larger for MACT ($R_{CT} \approx 1300\ \Omega$) compared to APC ($R_{CT} \approx 300\ \Omega$). Since electrolytic dealloying will occur under an applied potential of 0.55 V vs. Mg, EIS was also conducted at the dealloying potential of 0.55 V vs. Mg as shown in **Figure 1b**, where four consecutive scans are combined in a scatter plot. Here MACT

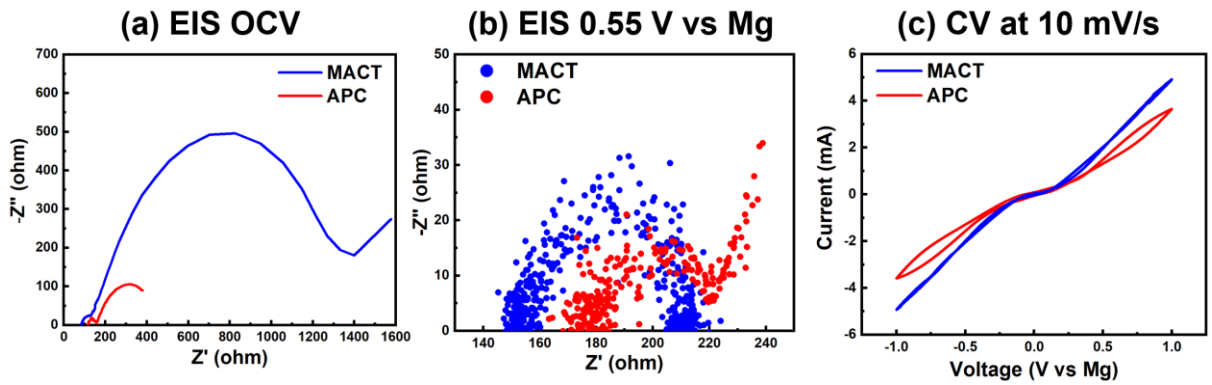

Figure 1. (a,b) *EIS comparing MACT and APC electrolytes at* ***(a)*** *OCV, and* ***(b)*** *0.55 V vs. Mg using scatter plot overlay of four consecutive scans;* ***(c)*** *Typical cyclic voltammetry tests from -1 to 1 V vs. Mg at 10 mV/s using symmetrical 1 cm^2 Mg electrodes.*

still has a lower R_Ω value of ≈154 Ω compared to ≈178 Ω for APC, but the values of R_{CT} are more comparable for APC and MACT. The impact of these resistive properties is seen in the CV performance of the cell. **Figure 1c** shows the typical CV collected between -1 to 1 V vs. Mg at the scan rate of 10 mV/s using symmetrical Mg electrodes with geometrical area of 1 cm^2 Mg in MACT (blue) and APC (red). Note that the current measured, which arises from Mg stripping (oxidation) and plating (reduction), is greater in MACT compared to APC for the symmetrical Mg cell at 0.2 V vs. Mg and higher. Thus, at the relevant dealloying potential of 0.55 V vs. Mg which has a sufficient overpotential to drive the reaction, MACT will be usable in electrolytic dealloying and may also have improved electrochemical performance due to its lower R_Ω value.

Next, we use both the APC and MACT electrolytes to dealloy Al-Mg parent alloys and create NP-Al. A parent alloy with composition $Al_{30}Mg_{70}$ at. % was created by melting the underlying Al and Mg at 850 °C using a tube furnace under argon flow. Before dealloying, the $Al_{30}Mg_{70}$ at. % parent alloy, which is very brittle, was crushed into coarse powder, and placed inside a stainless steel mesh pouch to use as the working electrode. (See Supplementary Information for more details on Experimental Methods.) The decision to use a powder increases the dealloying kinetics and reaction rate by increasing the surface area

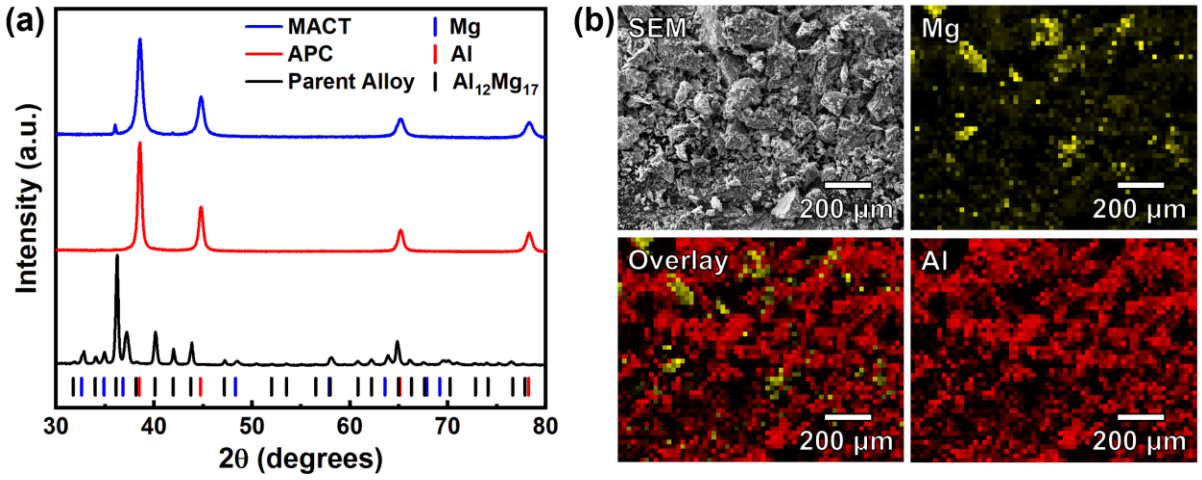

Figure 2. (a) *XRD characterization before and after dealloying for NP-Al samples created in APC and MACT electrolyte;* ***(b)*** *EDX mapping characterization of NP-Al sample created in MACT electrolyte after dealloying. (Al PDF # 01-085-1327, $Al_{12}Mg_{17}$ PDF # 01-073-1148, Mg PDF # 00-004-0770.)*

of the working electrode. This $Al_{30}Mg_{70}$ at. % composition is chosen because it contains two phases: hexagonal close-packed Mg and $Al_{12}Mg_{17}$ phases as shown by the black x-ray diffraction (XRD) curve in **Figure 2a**.[5] The reference and counter electrodes used are Mg foils, and the electrolyte used is APC or MACT to create two different types of NP-Al samples. During electrolytic dealloying, a voltage of 0.55 V vs. Mg is applied between the working and reference electrodes, which causes Mg to be removed from the working electrode and plated onto the Mg foil counter electrode. This stripping of Mg leaves behind NP-Al at the working electrode. The corresponding XRD of NP-Al is shown in **Figure 2a** by the blue and red curves for MACT and APC respectively. After removing Mg from the parent alloy, both samples have face-centered cubic Al as the remaining dominant phase. However, the MACT sample still has a small peak around $2\theta \approx 36°$ indicating residual $Al_{12}Mg_{17}$. Energy dispersive x-ray spectroscopy (EDX) was also used to characterize the elemental composition of the NP-Al samples. A composition of 97 at. % Al and 3 at. % Mg was detected for the APC sample, while a composition of 85 at. % Al and 15 at. % Mg was detected for the MACT sample. Further characterization of the elemental composition for the MACT sample via EDX mapping is shown in **Figure 2b** with Al in red and Mg in yellow. Note that this sample is not fully homogeneous regarding the distribution of Al and Mg concentrations after dealloying; most regions in EDX mapping are Al-rich in red (EDX: 94 at. % Al, 6 at. % Mg), while some residual Mg-rich regions in yellow are detected (EDX: 44 at. % Al, 56 at. % Mg). These two types of regions (i.e., Al-rich, and Mg-rich regions) balance to bring the EDX of the total region to 85 at. % Al and 15 at. % Mg as mentioned above. The residual Mg-rich regions observed after dealloying can be justified by the presence of partially dealloyed powder particles, caused by the relatively large size of some powder particles (by the time small particles are nearly fully dealloyed, large particles are not), in combination with the finer nature of the NP-Al created in MACT electrolyte (as will be discussed in the next section), which makes it difficult for dissolved Mg to diffuse out of the bulk of parent materials with large particle size. Since these Mg-rich regions are highly localized, the residual Mg does not impact the overall performance of the NP-Al material.

To characterize the structure size of the NP-Al, scanning electron microscopy (SEM), transmission electron microscopy (TEM), and small-angle X-ray scattering (SAXS) are used as shown in **Figure 3**. Here SEM shows the nanoporous morphology of the NP-Al samples made in the APC and MACT electrolytes

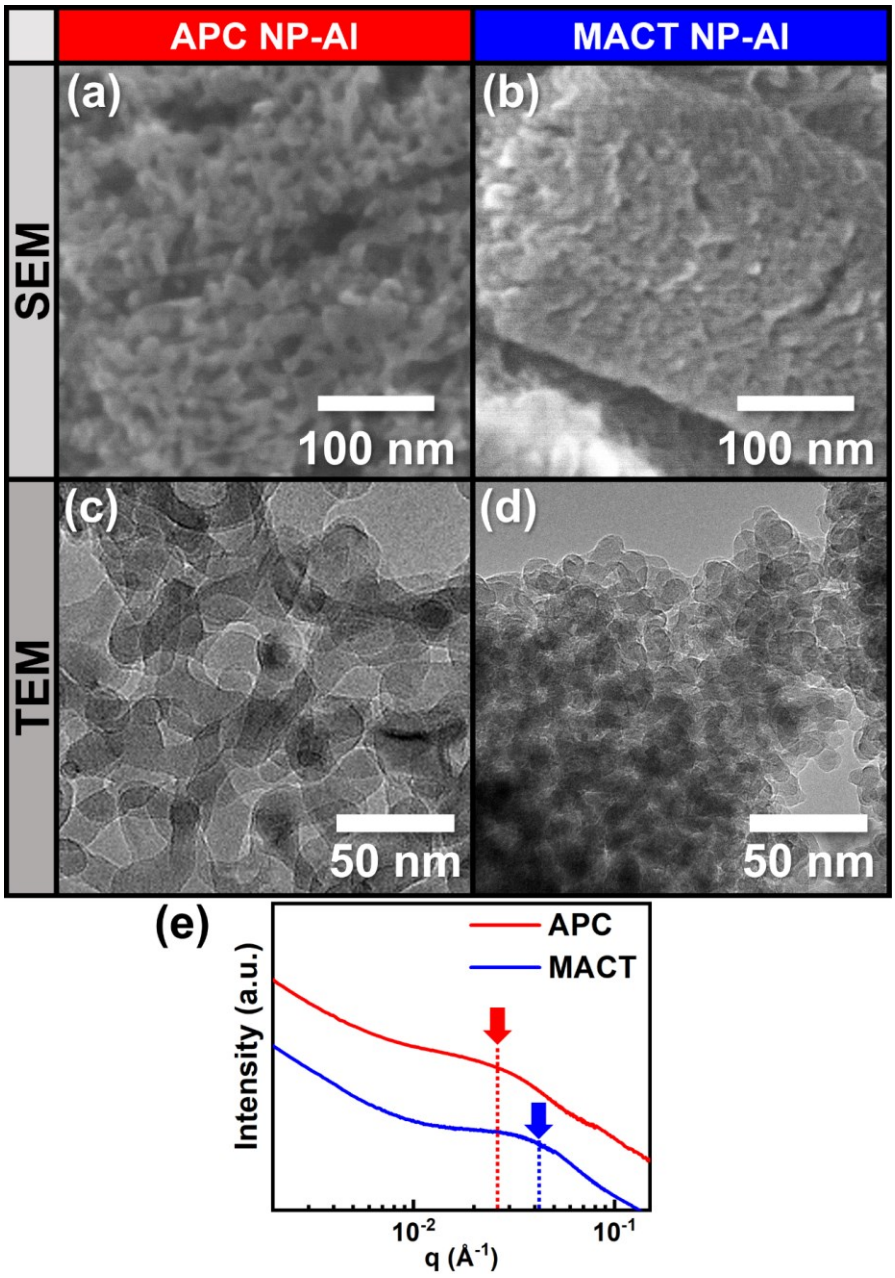

Figure 3. *Nanostructural characterization showing* ***(a-b)*** *SEM of NP-Al samples created in APC and MACT respectively, and* ***(c-d)*** *TEM of NP-Al created in APC and MACT respectively.* ***(e)*** *SAXS data with estimated peak* q_{max} *values identified by dotted lines and arrows.*

in **Figure 3a-b**. The pores of NP-Al made in MACT are visibly smaller than those for NP-Al made in APC. Higher magnification to examine the ligaments using TEM is shown in **Figure 3c-d**. For NP-Al made in APC, the typical dealloyed nanoporous structure with bicontinuous and well-defined ligaments and pores is observed; this is similar to other types of dealloyed systems like nanoporous gold [13,16] and matches previous NP-Al structures dealloyed in APC as well.[5] However, the NP-Al ligaments and pores appear to be smaller or finer in the MACT sample. To estimate the ligament size, ImageJ software was used on TEM images for both APC and MACT samples as shown in **Figure S1**. Here the ligament size for the APC sample is ≈10-20 nm in agreement with previous results[5], while the ligament size for MACT samples is smaller at ≈6-14 nm. To analyze the ligament structure size in a more quantitative way, SAXS is used as shown in **Figure 3e**. Note that SAXS measurements give a more comprehensive overview of the morphology of the entire sample compared to microscopy since the probed area in SAXS here is 2 mm^2, which is larger than the typical 0.04 μm^2 area viewed in TEM. Here we see in SAXS that the peak denoting the averaged distance between ligaments shifts to higher q values when comparing NP-Al created in APC versus MACT. This means that the averaged distance between NP-Al ligaments d in the MACT sample is smaller than that of the APC sample given the approximate relationship for dealloyed nanoporous structures used in **Eq. 1**[16,17]:

$$q_{max} \approx 1.23\frac{2\pi}{d} \qquad (\boldsymbol{Eq.\,1})$$

Here q_{max} is estimated for NP-Al created in APC and MACT as ≈0.026, and ≈0.042 $Å^{-1}$ denoted by the red and blue vertical dotted lines respectively, which corresponds to an averaged distance d between ligaments of ≈30 nm for APC (corresponding to ≈15 nm ligament sizes) and ≈18 nm for MACT (≈9 nm ligament sizes).[16,17] Thus, much smaller ligament and pore sizes can be achieved by switching from APC to MACT electrolytes for electrolytic dealloying.

After compositional and morphological characterization of both NP-Al samples, we reexamine some of the main advantages of electrolytic dealloying for the MACT sample. First, the recovery of the sacrificial component in dealloying is important for sustainable and practical applications.[18] Here we show recovery of Mg at the counter electrode in **Figure 4a-b** using both APC and MACT electrolytes. Interestingly, APC recovered Mg exhibits a solid, single formation, while MACT recovered Mg is in the form of a dark gray, loose powder. XRD analysis in **Figure 4c** of the two types of recovered Mg at the counter electrode (CE) show a pure Mg phase for samples created in both electrolytes, albeit a more crystalline result for APC is noticed compared to MACT. Furthermore, the microstructure of the MACT recovered Mg powder was analyzed and shown in **Figure S2**. Here ligament sizes can be seen on the order of 50-200 nm. Because of the nanoscale feature size of the Mg powder recollected at the counter electrode, there may be some other possible applications for this value-added byproduct that can potentially increase the productivity of electrolytic dealloying in MACT via synthesis of two desired products.

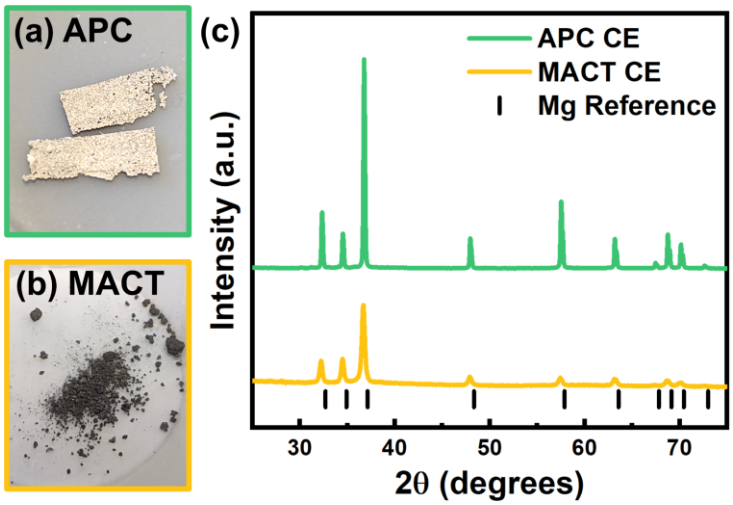

Figure 4. *Mg recovery process after dealloying showing* ***(a)*** *solid Mg from APC,* ***(b)*** *powder Mg from MACT, and* ***(c)*** *XRD characterization of both recovered Mg forms*

Finally, the high reactivity of NP-Al made in MACT is investigated by reacting it with DI H_2O as shown in **Figure 5**. The reaction chamber used is kept under argon, and the water is sparged with argon for 15 minutes prior to the reaction to remove oxygen as an oxidizer. Immediately upon reaction, a large metal fire occurs between NP-Al made in MACT and H_2O as shown in **Figure 5a-c** and **Video S1**. After the first 5 minutes of the reaction, the entire solid sample is collected via filtration as shown in **Figure 5d**. Here several solid white reaction byproducts are observed (orange circles). When analyzing these white

byproducts by XRD in **Figure 5e** (orange curve), we detect the Al phase from unreacted NP-Al and various α-, γ-, or η-phases of Al_2O_3. Meanwhile, when NP-Al made in APC reacts with DI H_2O for 3 days, no large metal fire is observed in the initial reaction as shown in **Video S1**, where hydrogen is released and collected relatively slowly and bayerite $Al(OH)_3$ is detected (purple curve).[19] In the reaction between Al and H_2O, three types of reactions are possible based on the experimental conditions:

$$2Al + 6H_2O \xrightarrow{<280°C} 2Al(OH)_3 + 3H_2 + heat \quad (\boldsymbol{Eq.2})$$

$$2Al + 4H_2O \xrightarrow{280-480°C} 2AlO(OH) + 3H_2 + heat \quad (\boldsymbol{Eq.3})$$

$$2Al + 3H_2O \xrightarrow{>480°C} Al_2O_3 + 3H_2 + heat \quad (\boldsymbol{Eq.4})$$

Note that heat is released because all 3 of these reactions are highly exothermic and that some or all reactions may occur to varying degrees due to varying high temperatures reached from exothermic self-heating.[20,21] To produce the Al_2O_3 phases detected in the NP-Al byproduct, the Al-containing byproducts bayerite $Al(OH)_3$ and boehmite AlO(OH) from **Eq.2** and **Eq. 3** can convert to η- and γ-phases of Al_2O_3 respectively from ≈300-600°C,[22,23] while α-Al_2O_3 is formed at very high temperatures above 1100°C (although some reports have shown nanocrystalline α-Al_2O_3 can form at as low as 300-400°C under certain circumstances).[21,23] We hypothesize that this wet oxidation reaction creating Al_2O_3, which becomes self-supported from the large exothermic reaction noticed, only occurs for the NP-Al created in MACT but not for the NP-Al created in APC due to the finer nanoporous structure observed with smaller ligament sizes of the NP-Al created in MACT. Further optimization of reaction parameters such as the amount of NP-Al powder, amount of water, or even the size and shape of container used can further improve the exothermic self-heating and the yield for Al_2O_3 formation via **Eq. 4**. Such optimization would be preferable to increase the wet capacity of hydrogen in respect to aluminum and water, which is 3.73 wt. % for **Eq. 2** and 5.60 wt. % for **Eq. 4**. Furthermore, a faster reaction may occur for **Eq. 4** as the full yield for **Eq. 2** can take several days to occur.[19] Thus, further studies optimizing the reaction of NP-Al created in MACT with water or other strong oxidizers can unlock potential applications for rapid oxidation of Al and release of hydrogen for high-power fuel purposes like for space propulsion.[24]

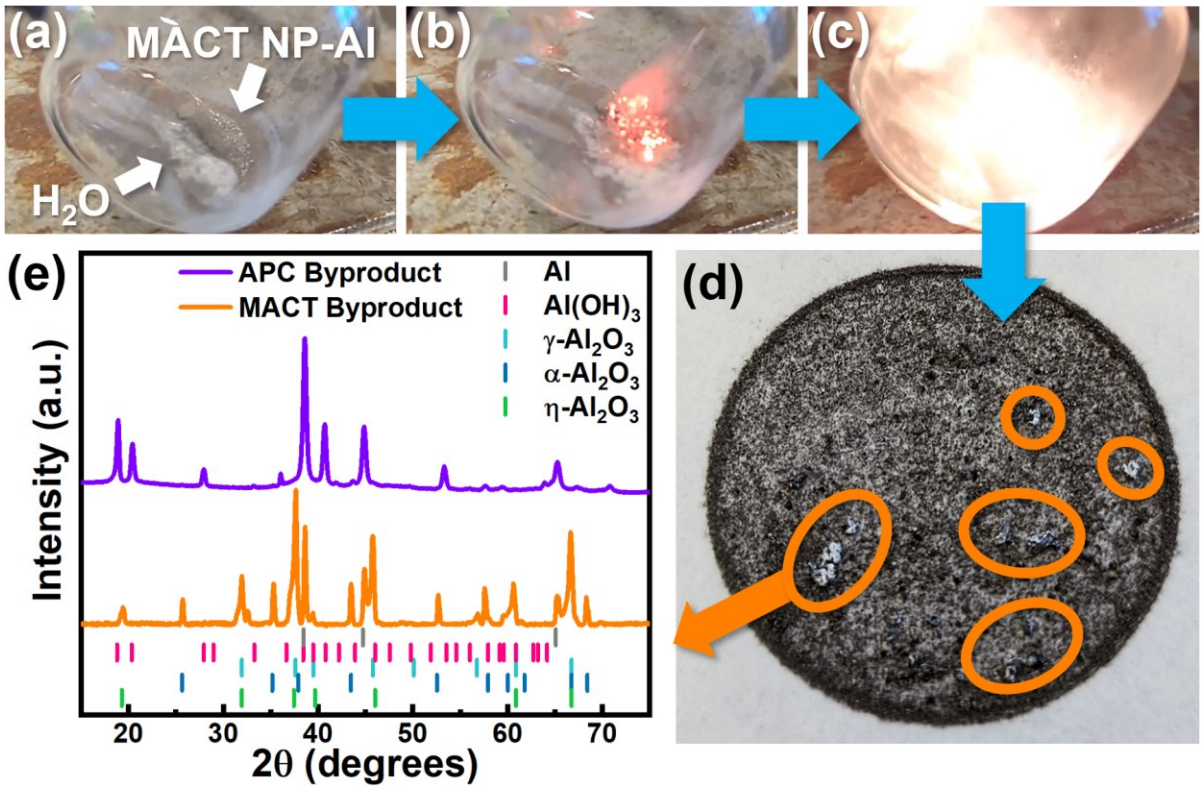

Figure 5. (a-c) *Reaction between NP-Al created in MACT and DI H_2O showing development of initial fire;* ***(d)*** *collection of all solid byproduct after 5 minutes with some white byproducts circled in orange;* ***(e)*** *XRD of byproducts from reaction of NP-Al created in APC (purple curve, after 3 days) and MACT (orange curve, after 5 minutes) with water. ($Al(OH)_3$ PDF # 00-012-0457, γ-Al_2O_3 PDF # 00-002-1420, α-Al_2O_3 PDF # 00-001-1243, η-Al_2O_3 PDF # 00-004-0875.)*

In conclusion, NP-Al can be synthesized by using an alternative electrolyte besides APC such as MACT, which improves the versatility of the electrolytic dealloying method. At the applied relevant dealloying potential of 0.55 V vs. Mg, MACT exhibits better electrochemical performance than APC and can be used to synthesize a finer nanoporous structure with ligament sizes ≈6-14 nm. Furthermore, the advantages of electrolytic dealloying remain present. Sacrificial Mg used during dealloying in MACT electrolyte to create NP-Al can also be recovered, thus making this synthesis method more sustainable and practical for scaling purposes. Finally, the high reactivity of finer NP-Al created in MACT exhibited by its exothermic reaction

with DI H_2O produces a large amount of heat that can form various phases of Al_2O_3, thus warranting further exploration on the application of NP-Al created in MACT for high-power fuel purposes.

Acknowledgments

The authors are thankful to the National Science Foundation (NSF) for their financial support via NSF-CAREER (Award Number: CMMI-2047851, Eric Detsi) and NSF GRFP (Award Number: DGE-1845298, Timothy Lee). The authors acknowledge use of the Dual Source and Environmental X-ray Scattering facility operated by the Laboratory for Research on the Structure of Matter at the University of Pennsylvania (NSF MRSEC 17-20530). The equipment purchase was made possible by an NSF MRI grant (17-25969), an ARO DURIP grant (W911NF-17-1-0282), and the University of Pennsylvania. This work was carried out in part at the Singh Center for Nanotechnology, part of the National Nanotechnology Coordinated Infrastructure Program, which is supported by the NSF grant NNCI-1542153.

References

[1] J. Fu, Z. Deng, T. Lee, J.S. Corsi, Z. Wang, D. Zhang, E. Detsi, ACS Appl. Energy Mater. 1 (2018) 3198–3205.

[2] C. Wang, G. Zhu, P. Liu, Q. Chen, ACS Nano 14 (2020) 2404–2411.

[3] I.V. Okulov, S. V. Lamaka, T. Wada, K. Yubuta, M.L. Zheludkevich, J. Weissmüller, J. Markmann, H. Kato, Nano Res. 11 (2018) 6428–6435.

[4] S. Liu, X. Bian, J. Liu, J. Wang, M. Yu, Y. Yang, R. Fan, Intermetallics (2018).

[5] J.S. Corsi, J. Fu, Z. Wang, T. Lee, A.K. Ng, E. Detsi, ACS Sustain. Chem. Eng. 7 (2019) 11194–11204.

[6] G. Han, J.H. Um, H. Park, K. Hong, W.S. Yoon, H. Choe, Scr. Mater. (2019).

[7] W. Yang, X.-G. Zheng, S.-G. Wang, H.-J. Jin, J. Electrochem. Soc. 165 (2018) C492–C496.

[8] T. Lee, J.S. Corsi, L. Wang, E. Detsi, ACS Appl. Energy Mater. (2021).

[9] O. Mizrahi, N. Amir, E. Pollak, O. Chusid, V. Marks, H. Gottlieb, L. Larush, E. Zinigrad, D. Aurbach, J. Electrochem. Soc. (2008).

[10] H. Yaghoobnejad Asl, J. Fu, H. Kumar, S.S. Welborn, V.B. Shenoy, E. Detsi, Chem. Mater. (2018).

[11] T. Gao, F. Han, Y. Zhu, L. Suo, C. Luo, K. Xu, C. Wang, T. Gao, F. Han, Y. Zhu, L. Suo, C. Luo, C. Wang, K. Xu, Adv. Energy Mater 5 (2015) 1401507.

[12] L. Yang, C. Yang, Y. Chen, Z. Pu, Z. Zhang, Y. Jie, X. Zheng, Y. Xiao, S. Jiao, Q. Li, D. Xu, ACS Appl. Mater. Interfaces 13 (2021) 30712–30721.

[13] J. Erlebacher, M.J. Aziz, A. Karma, N. Dimitrov, K. Sieradzki, Nature (2001).

[14] E. Rouya, S. Cattarin, M.L. Reed, R.G. Kelly, G. Zangari, J. Electrochem. Soc. 159 (2012) K97–K102.

[15] Y. Xie, C. Li, E. Castillo, J. Fang, N. Dimitrov, Electrochim. Acta 385 (2021) 138306.

[16] C. Soyarslan, S. Bargmann, M. Pradas, J. Weissmüller, Acta Mater. 149 (2018) 326–340.

[17] A.K. Ng, S.S. Welborn, E. Detsi, Scr. Mater. 206 (2022) 114215.

[18] J.S. Corsi, J. Fu, L. Wang, S. Welborn, Z. Wang, E. Detsi, J. Electrochem. Soc. (2022).

[19] T. Lee, J. Fu, V. Basile, J.S. Corsi, Z. Wang, E. Detsi, Renew. Energy 155 (2020) 189–196.

[20] US DOE, Reaction of Aluminum with Water to Produce Hydrogen, 2008.

[21] A. V. Bersh, A. V. Lisitsyn, A.I. Sorokovikov, M.S. Vlaskin, Y.A. Mazalov, E.I. Shkol'Nikov, High Temp. 2010 486 48 (2010) 866–873.

[22] M.S. Vlaskin, A. V. Grigorenko, A.Z. Zhuk, A. V. Lisitsyn, A.E. Sheindlin, E.I. Shkol'nikov, High Temp. (2016).

[23] O. V. Al'myasheva, E.N. Korytkova, A. V. Maslov, V. V. Gusarov, Inorg. Mater. (2005).

[24] F. Maggi, S. Dossi, C. Paravan, L.T. DeLuca, M. Liljedahl, Powder Technol. 270 (2015) 46–52.